Electronic Supplementary Information

Disentangling Size Effects and Spectral Inhomogeneity in Carbon Nanodots by Ultrafast Dynamical Hole-Burning

Alice Sciortino,[a,b,c] Michela Gazzetto,[c] Gianpiero Buscarino,[a,d] Radian Popescu,[e] Reinhard Schneider,[e] Gaetano Giammona,[f] Dagmar Gerthsen,[e] Egmont J. Rohwer,[c] Nicolò Mauro,[f] Thomas Feurer,[c] Andrea Cannizzo,[c] and Fabrizio Messina [a,d]

[a.] *Dipartimento di Fisica e Chimica, Università degli Studi di Palermo, Via Archirafi 36, 90123 Palermo, Italy. Email: fabrizio.messina@unipa.it*
[b.] *Dipartimento di Fisica e Astronomia, Università degli studi di Catania, Via Santa Sofia 64, 95123 Catania, Italy.*
[c.] *Institute of Applied Physics, University of Bern, Sidlerstrasse 5, CH-3012 Bern, Switzerland. Email: andrea.cannizzo@iap.unibe.ch*
[d.] *CHAB-ATeN Center, Università degli studi di Palermo, Viale delle Scienze, Edificio 18, 90128 Palermo, Italy.*
[e.] *Laboratory for Electron Microscopy, Karlsruhe Institute of Technology, Engesserstrasse 7, 76131 Karlsruhe, Germany.*
[f.] *Dipartimento di Scienze e Tecnologie Biologiche, Chimiche e Farmaceutiche (STEBICEF), Università degli Studi di Palermo, Via Archirafi 32, 90123 Palermo, Italy.*

Data reduction and Analysis procedures

a) TA data:

The TA data presented in the paper were obtained by averaging the results of 10-20 successive scans, each typically spanning 100 time delays from t=0 to t=300 ps. Following standard procedures,[S1] the data were corrected by the effect of group velocity dispersion (GVD), cross-phase modulation (XPM) and pump scattering. In particular, cross-phase modulation between pump and probe pulses introduces artifacts that strongly distort the signal collected within a time window of duration 280 fs around time zero. These data were removed from all the datasets reported in the paper. Strong scattering of the pump affects the data collected in a spectral window of about 20 nm around the central pumping wavelength, which were cut out before any further analysis. In order to increase the signal-to-noise ratio, the data were processed by eliminating highest order contributions (n>10) as obtained by a singular value decomposition (SVD) analysis.[S1]

To calculate the anisotropy *r* shown in Figure 2h, we performed TA experiments in parallel and in perpendicular polarization between pump and probe and we used the following formula:[S2]

$$r = \frac{I_{\parallel} - I_{\perp}}{I_{\parallel} + 2\,I_{\perp}}$$

In which $I_{\parallel/\perp}$ represents the TA signal (at the wavelength of interest) measured in parallel and perpendicular polarization respectively.

To isolate the ground state bleaching in the TA spectra, as shown in Fig. 3, a subtraction of the stimulated emission contribution was performed, by comparing it with the spontaneous emission signal recorded in the steady state experiments. Because these two types of emission depend on different processes and to make them comparable it is necessary to multiply the spontaneous emission L(λ) for λ^4.

The anaylsis of the TA spectra reported in Figure S6 was carried out via a global analysis approach using the SVD method, and performing a multiexponential global fit (GF) of the kinetic traces extracted from the procedure. The global analysis leads to factorize the signal separating the temporal from the spectral dependence, and to fit it with the following function:

$$\sum_i A_i(\lambda) \exp\left(-\frac{t}{\tau_i}\right) \cdot \mathrm{u(t)} \times IRF(t)$$

in which the time constants are a common parameters at all wavelengths, the amplitudes A_i are defined for each wavelength and called DAS, a step function is used to define the excitation time, the whole function is convoluted the instrumental response function (IRF) of the instrument, a Gaussian function of 130 fs full width at half maximum.

b) HRTEM data:

HRTEM images of single CDs were evaluated by calculating their two-dimensional Fourier transform (FT) pattern, which yields information on the crystal structure (lattice parameters and crystal symmetry). The analysis was performed by comparing the experimental FTs and calculated diffraction pattern, obtained by using the Jems (Java version of the electron microscopy simulation) software.[S3] All Bragg reflections are marked and indexed in FTs by using light-blue circles, while the zero-order beam (ZB) is indicated by a white circle.

Supplementary Figures and Tables

Table S1. Fit parameters of the curves in Fig. 3b reproducing the GSB and ESA signal vs λ_{exc}. The accuracy on the peak position and on the FWHM is 0.05 eV. Δ_{12} is separation between the two peaks

	GSB		ESA		
λ_{exc} (nm)	Peak (eV)	FWHM (eV)	Peak (eV)	FWHM (eV)	Δ_{12} (eV)
495	2.56 (484 nm)	0.42	3.00 (413 nm)	0.76	0.44
520	2.47 (502 nm)	0.40	2.91 (428 nm)	0.83	0.44
537	2.35 (528 nm)	0.38	2.70 (459 nm)	0.80	0.35
554	2.30 (539 nm)	0.38	2.67 (464 nm)	0.90	0.37
570	2.22 (558 nm)	0.37	2.65 (468 nm)	0.86	0.43

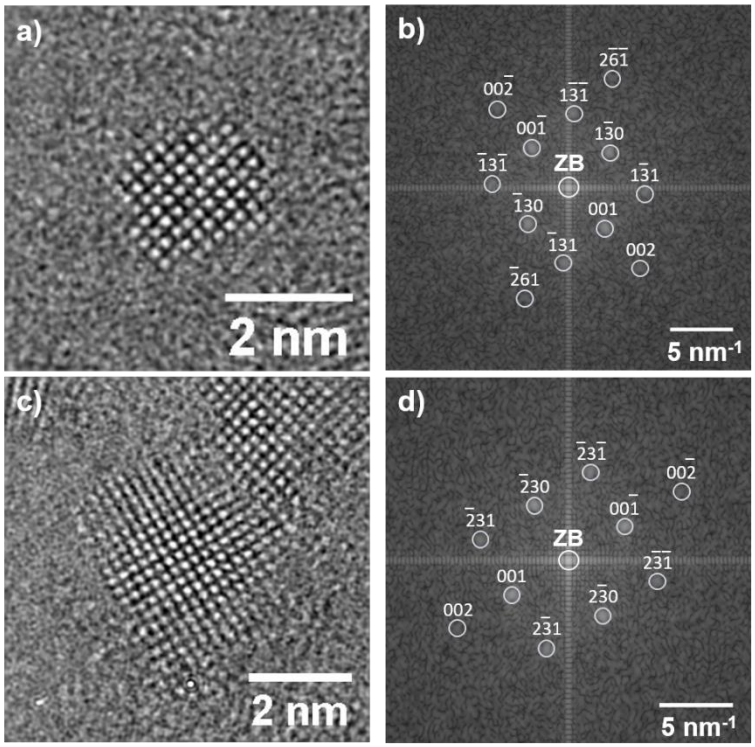

***Figure S1*:** HRTEM images of two *CDs* (a,c) and their corresponding 2-dimensional Fourier transform patterns (b, d). Each *CD* consists in a single β-C_3N_4 monocrystal with a hexagonal structure, as indicated by the good agreement between its Fourier transform and the calculated diffraction pattern of the bulk hexagonal β-C_3N_4 (space group P63/m, space group number 176 with lattice parameters of a=b=6.38 Å, and c=2.395 Å[S4]) in the [310] *(b)* and [320] *(d)* zone axis.

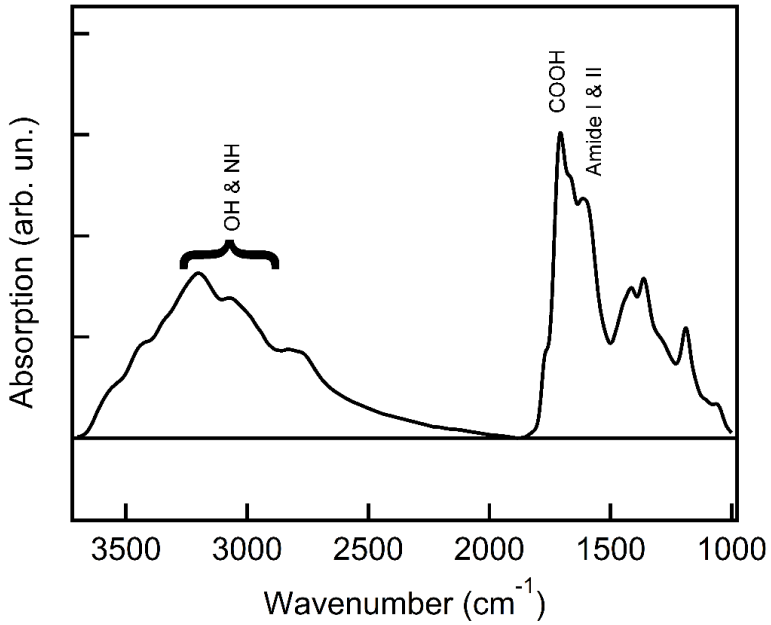

Figure S2: Typical infrared absorption spectrum of CDs. The labels indicate attributions we propose for the observed absorption peaks. The main vibrational signals associated to the surface structure of these CDs are due to amide (~1670-1600 cm^{-1}), carboxylic groups (1700 cm^{-1}) and hydroxyl groups (~3200 cm^{-1}).

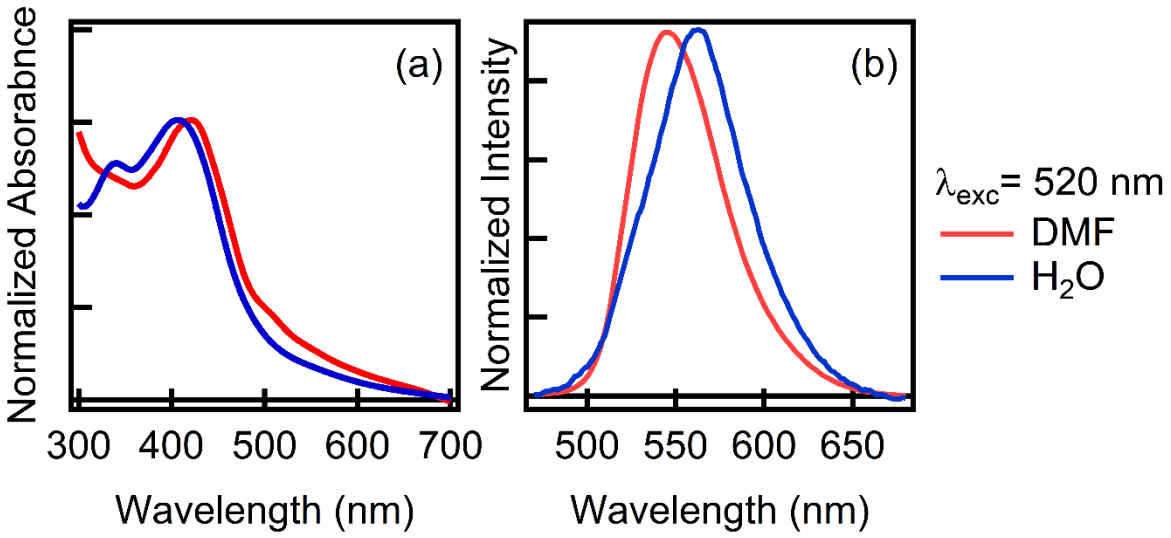

***Figure S3*:** (a) Absorption spectra of a solution of CDs dispersed in DMF (red) and in water (blue) with (b) the related emission spectrum recorded at 520 nm at the same concentration of CDs. The data clearly highlight the hydrogen bond-dependent solvatochromic behaviour of the electronic transition at long wavelengths. The latter is shown by the different oscillator strength in the two solvents (panel a), larger in aprotic DMF, and the associated solvatochromic shift of the fluorescence (panel b).

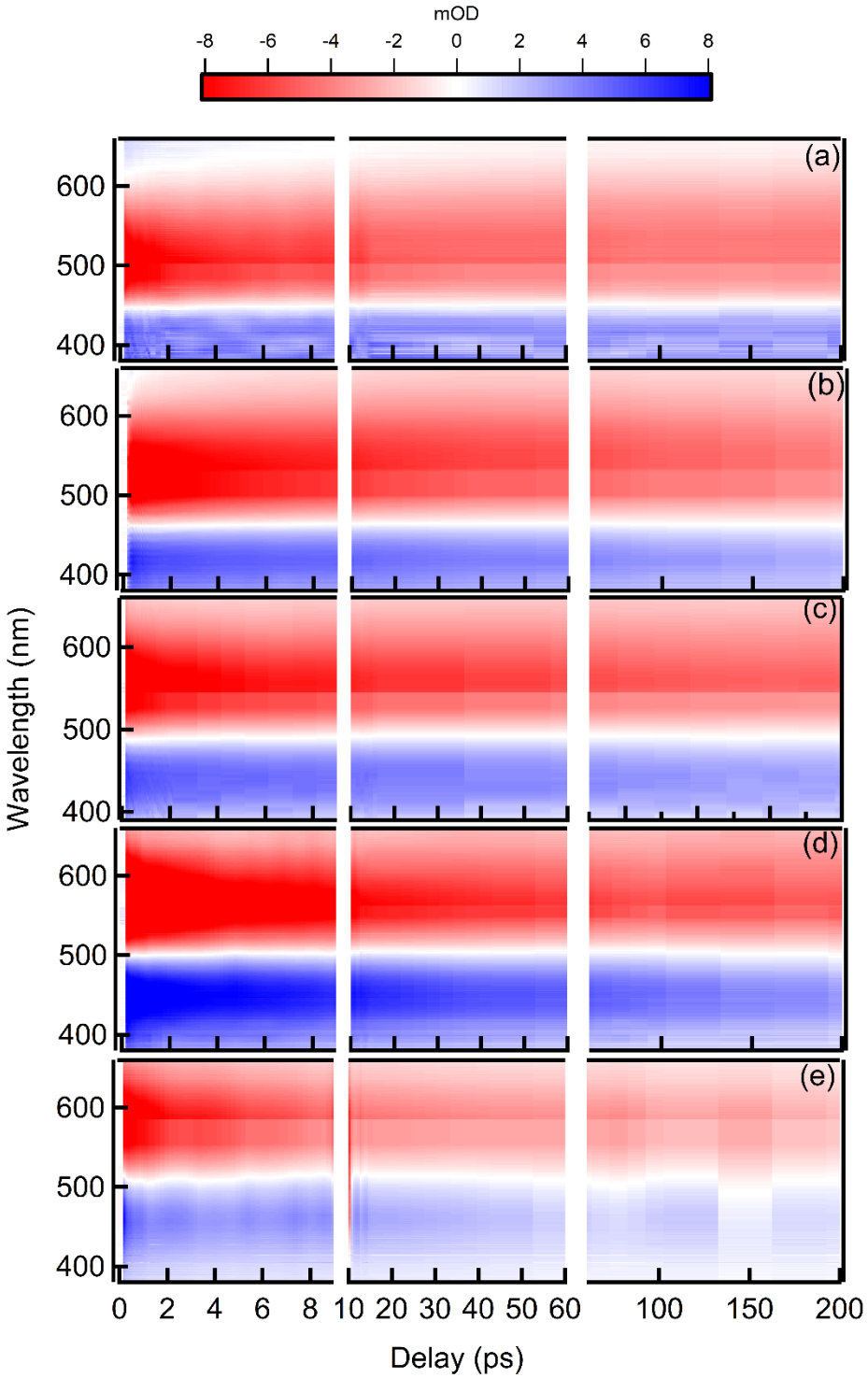

Figure S4: Complete two-dimensional time-wavelength plots of transient absorption measurements recorded with a pump wavelength of 495 nm (a), 520 nm (b), 537 nm (c), 554 nm (c) and 570 nm (d). The data are the same as in Fig. 2a-e, but shown here in a longer temporal range. These measurements were all performed at the same pump intensity and at magic angle polarization condition between pump and probe.

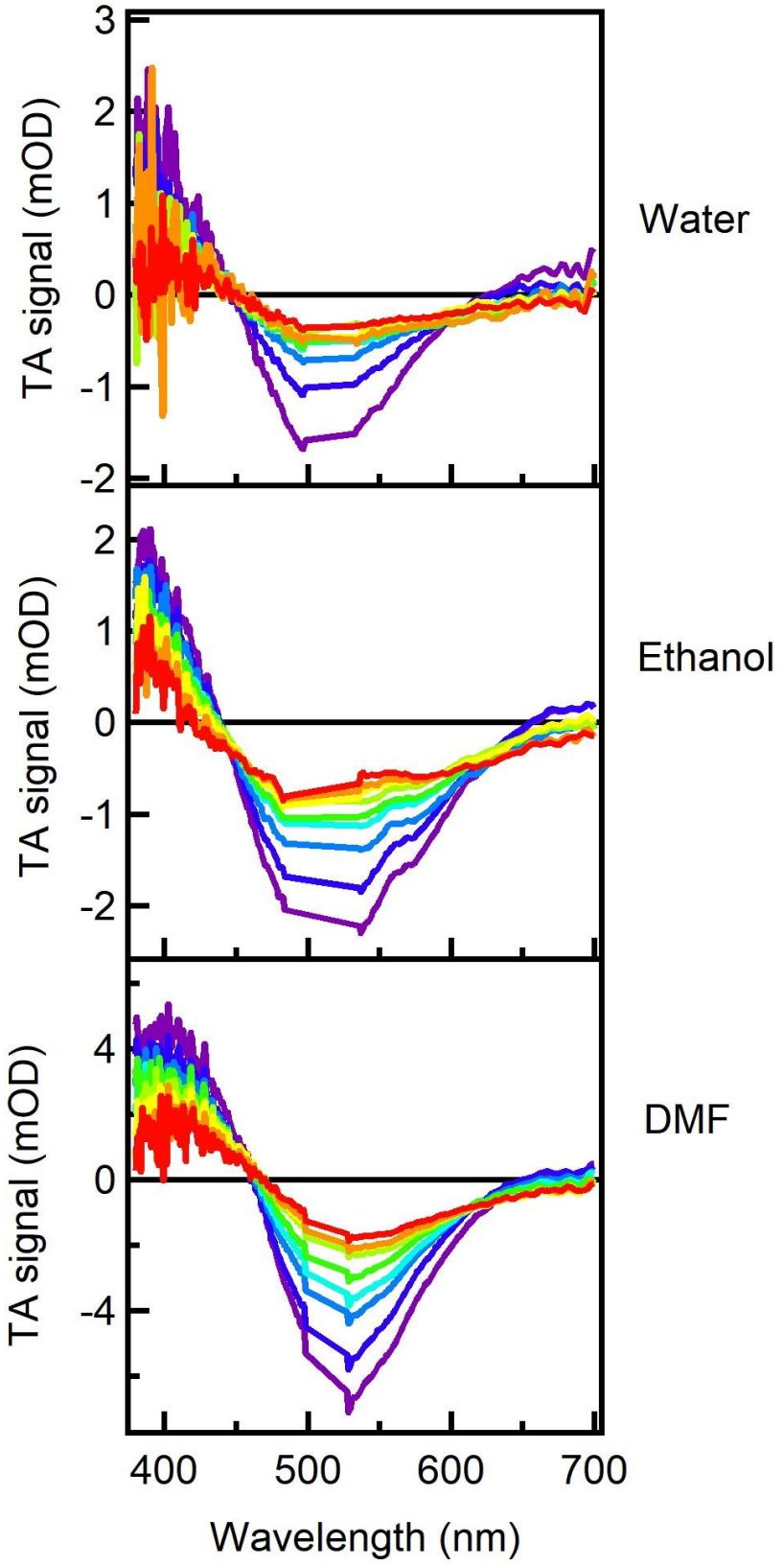

Figure S5: Transient absorption spectra recorded at 520 nm excitation of CDs solutions in different solvents, as recorded at different delays between pump and probe (from purple to red: 0.2 ps, 0.8 ps, 3 ps, 6 ps, 10 ps, 30 ps, 60 ps, 100 ps, 200 ps). Data were recorded at magic angle condition between pump and probe. In all solvents, we observe a clear decay of the signal over the entire spectral region. The region around 520 nm is removed because contaminated by the pump scattering.

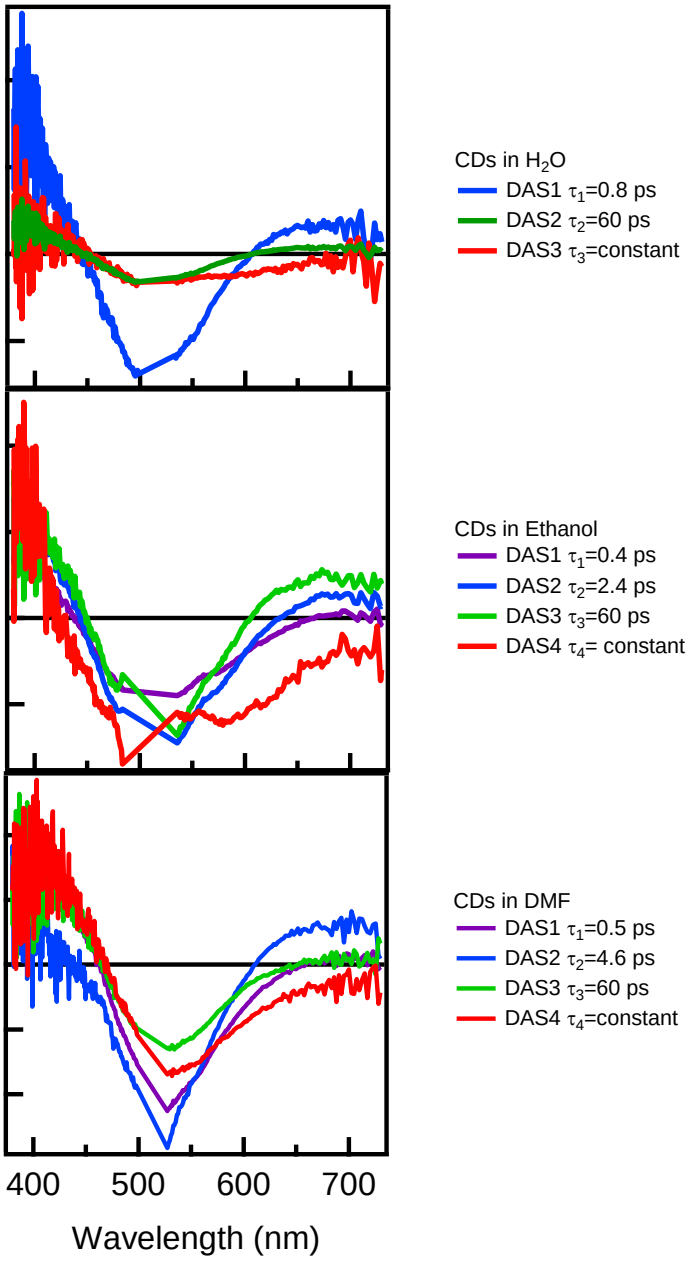

***Figure S6*:** Decay-associated spectra (DAS), and the respective characteristic times, as obtained with a global analysis by the SVD method[S1] of the TA data in different solvents reported in Figure S5. In each panel, the DAS associated with the shorter time scales (smaller than 10 ps) are attributed to solvation processes which drive a partial depopulation of the excited state, together with a redshift of the stimulated emission (as from the positive sign of the DAS at wavelengths > 600 nm); in fact, these time constants are solvent-dependent and consistent with the respective solvent response times. The DAS associated to the timescale of 60 ps describes an additional decay of the signal. The last DAS describes the nanosecond-lived signal, responsible of steady-state emission.

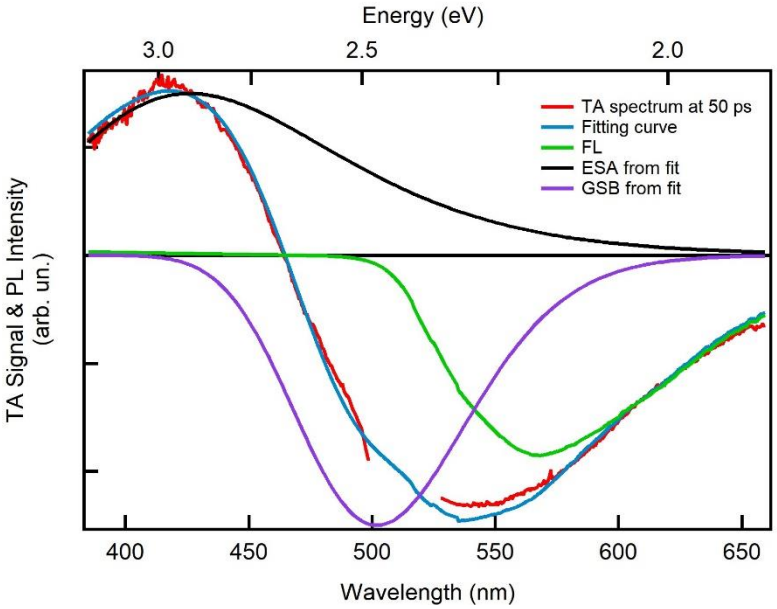

***Figure S7*:** TA spectrum of CDs in DMF recorded at 50 ps (red curve) overlapped with the best fitting curve (light blue curve) obtained by the sum of three signals: ESA (Gaussian black curve), GSB (Gaussian purple curve), as determined from a fit procedure, and fluorescence normalized spectrum (green curve), obtained experimentally.

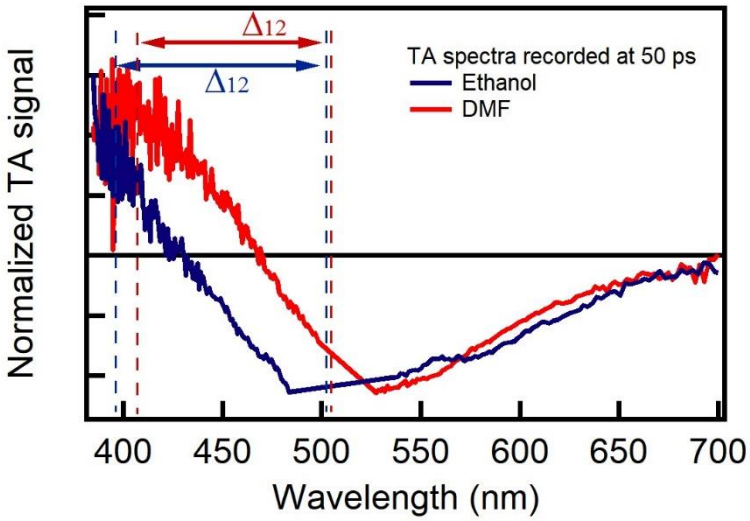

Figure S8: Normalized TA spectra recorded at 50 ps of a solution of CDs in ethanol (blue) and DMF (red), both excited at 520 nm. It is evident that the intensity ratio between ESA and GSB is independent of the solvent in which CDs are dissolved, although the spectral shift between the two signals depends on the proticity of the solvent.

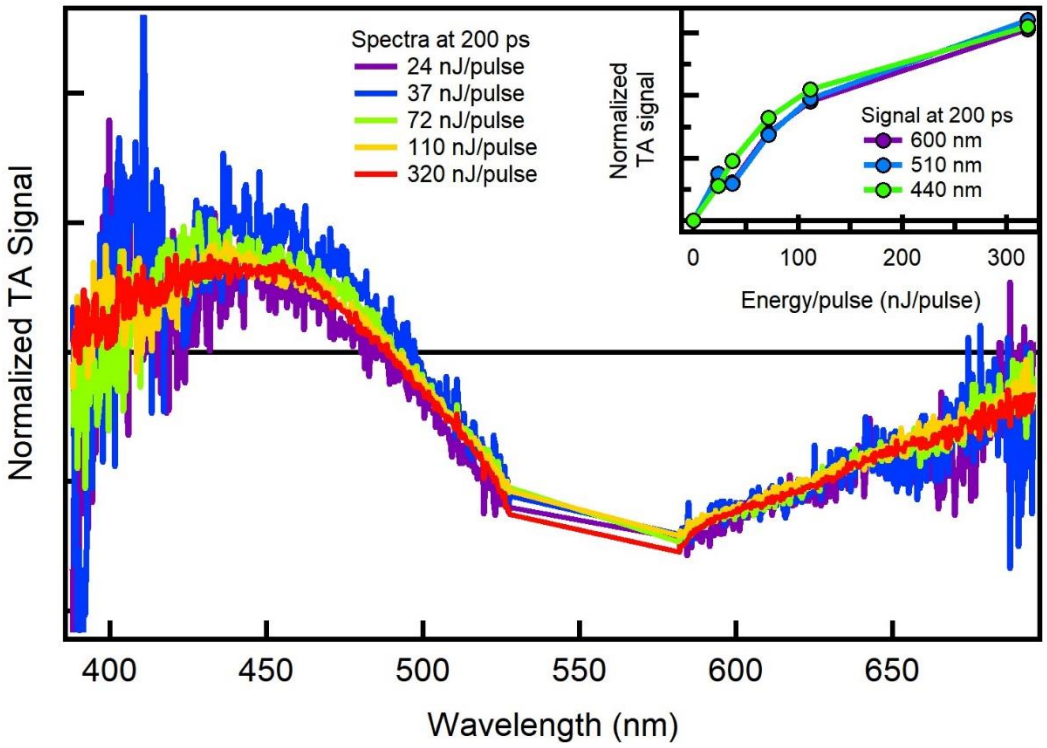

Figure S9: Normalized TA spectra recorded at t=200 ps of the same solution of CDs excited at 550 nm with different excitation intensities (indicated in the legend). Inset: the signal intensity at three different wavelengths as measured at different fluences. Increasing the excitation intensity saturates the electronic transition involved (as from the sublinear trend in the inset) but does not change the shape of the signal (as from the main panel).

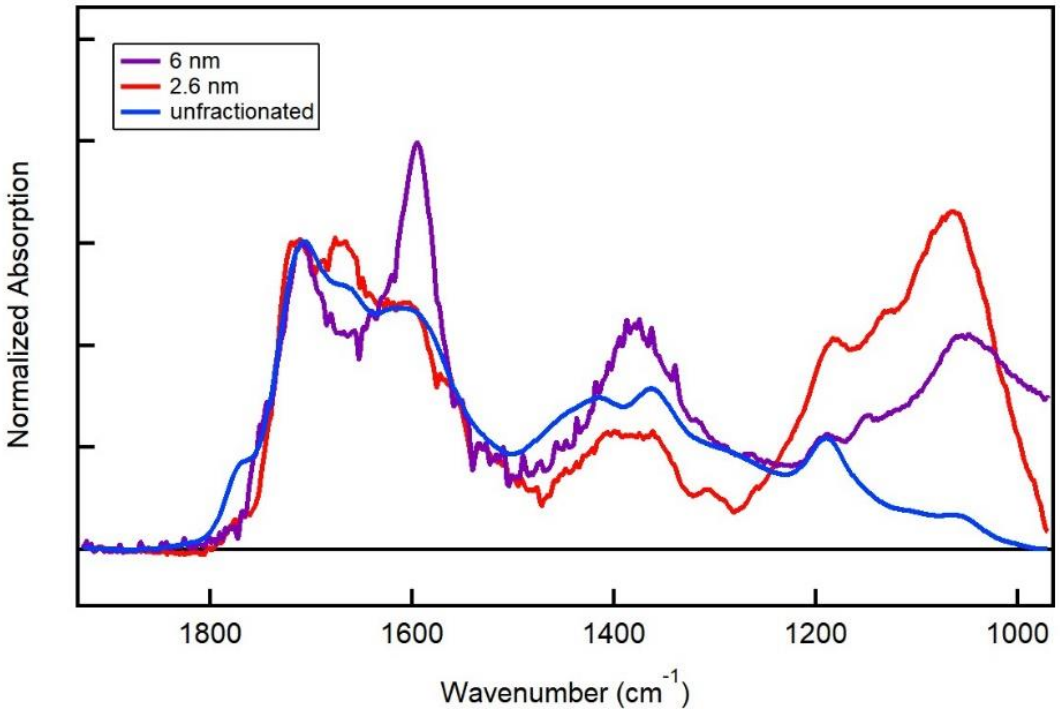

***Figure S10*:** FTIR measurements of differently-sized CD fractions obtained by SEC, compared with the unfractionated CD sample. The spectra display the usual complex pattern of vibrational fingerprints associated to the highly polyfunctional surfaces of CDs, similar to Figure S2. The spectra collected from the two fractions are similar: they contain the same vibrational fingerprints (e.g. C=O vibration around 1700 cm^{-1}, amide around 1600 cm^{-1}, C-N around 1400 cm^{-1}…), although in different relative ratios.

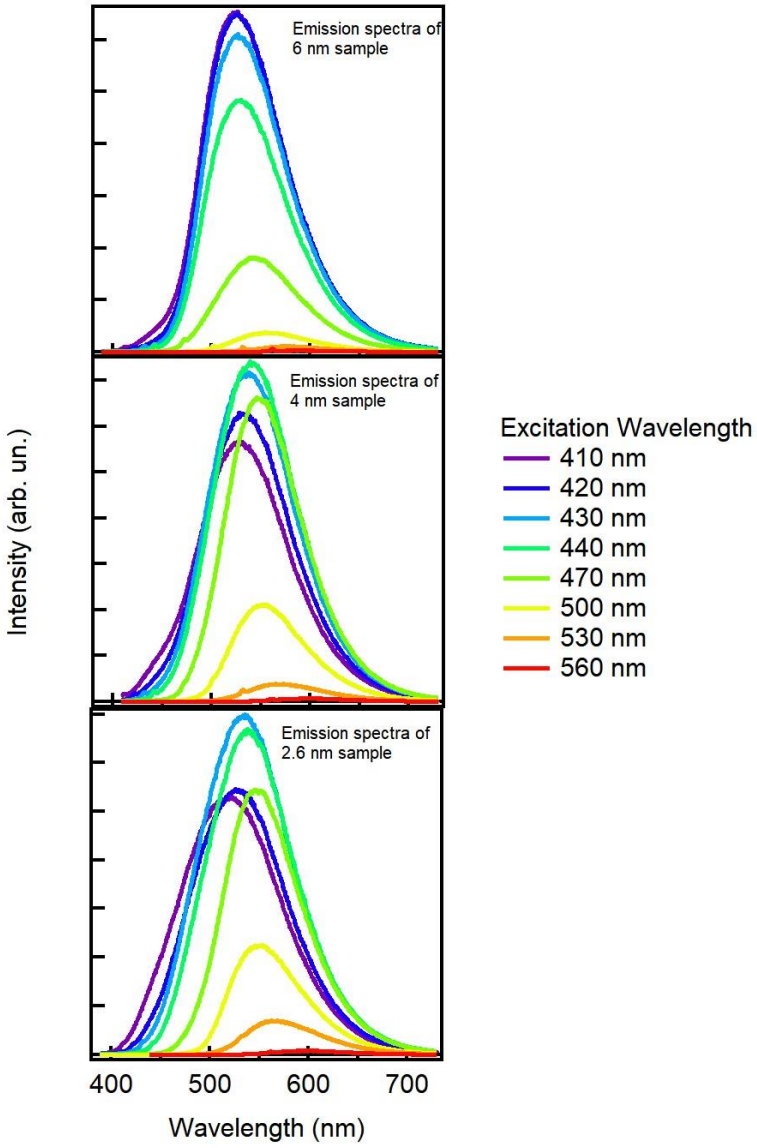

Figure S11: Emission spectra of the three subsets of CDs obtained by SEC. The excitation wavelength and the size of the samples are indicated in the legend.

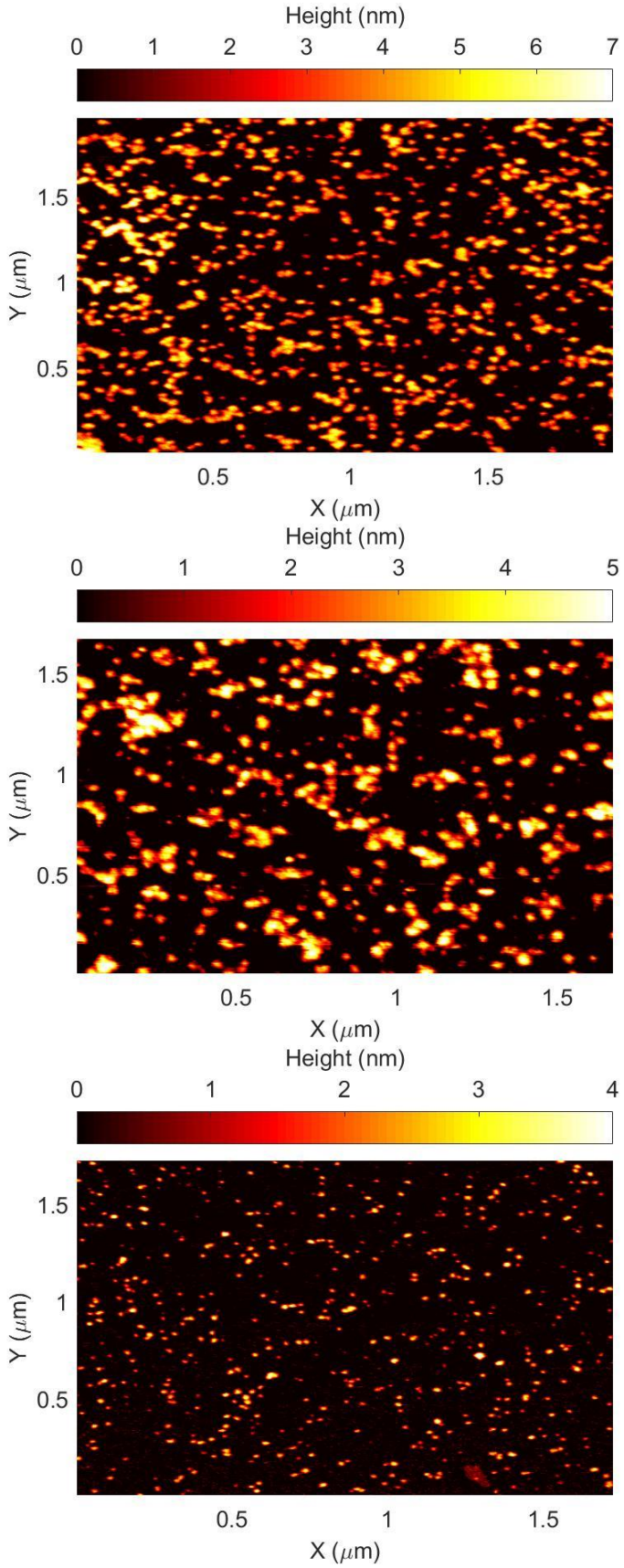

Figure S12: AFM measurement performed on the three subsets of CDs obtained by the SEC: 6 nm sample (top panel), 4 nm sample (middle panel), 2.6 nm sample (bottom panel). Each size distribution is obtained by sampling a few thousands of dots. The corresponding size distributions are reported in Figure 4a.

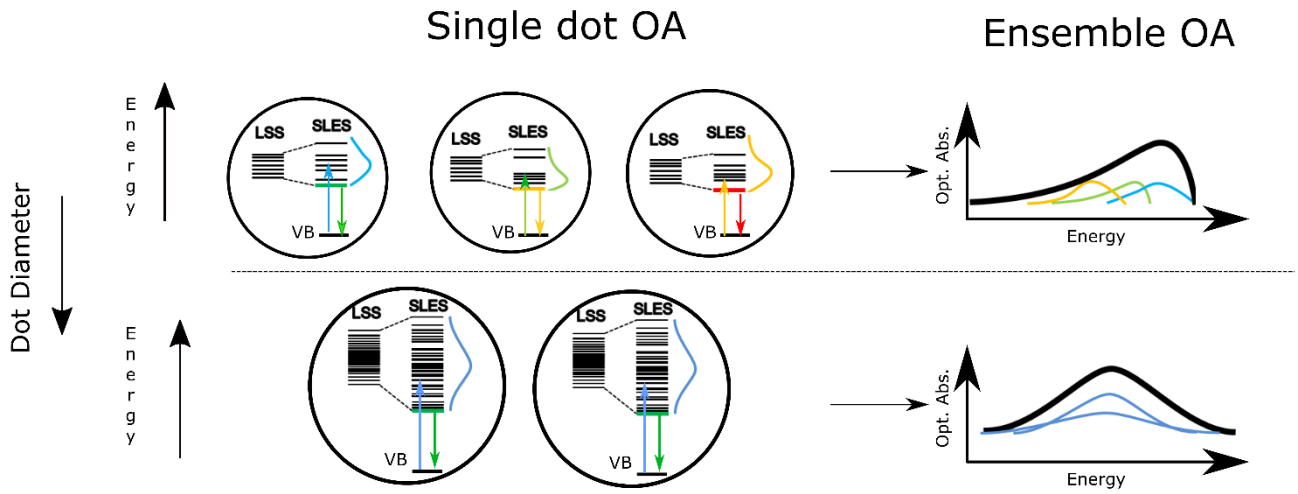

Figure S13: Graphical representation of the model proposed to explain the electronic properties of CDs in their low energy manifold. As represented in the Figure, the distribution of local surface states (LSS) on each CD and their mutual coupling determines the distribution of the surface localized exciton (SLEs) states. The latter ultimately controls the emission energy, because the emission occurs via a radiative recombination of the SLE, composed by a surface-localized electron and a hole left in the valence band (VB).[S5] In small dots (upper half of the Figure), the small number of LSS per dot, and their large surface-to-volume ratio both cause strong dot-to-dot variations of the energy structure. As a consequence, the absorption and emission energies of each dot are unique and widely fluctuating, explaining their large fluorescence tunability. The sum of all single dot absorption spectra yields the overall absorption spectrum at the ensemble level (right), very broad and highly asymmetrical. Large dots (lower half of the Figure) enter a statistical regime characterized by a large number of highly coupled LSS. In this case, dot-to-dot statistical fluctuations of the exciton energy become much smaller, and the ensemble OA absorption (lower right) becomes much narrower and Gaussian-like, with an increase of the homogeneous behaviour with respect to smaller dots.

References

[S1] C. Ruckebusch, M. Sliwa, P. Pernot, A. de Juan, and R. Tauler. *J. Photoch. Photobio. C*, 2012, **13**, 1-27

[S2] J. R. Lakowicz, *Principles of Fluorescence Spectroscopy – third edition*, **Springer**

[S3] http://www.jems-saas.ch/

[S4] M. Marqués, J. Osorio, R. Ahuja, M. Flórez, and J. M. Recio *Phys. Rev. B,* 2004, **70**, 104114

[S5] A. Sciortino, E. Marino, B. van Dam, P. Schall, M. Cannas, F. Messina, *J. Phys. Chem, Lett.* 2016, **7**, 3419-3423.